JOURNAL OF SYNCHROTRON RADIATION
ISSN 1600-5775

Influence of the core-hole effect on optical properties of magnesium oxide (MgO) near the Mg *L*-edge region

Mangalika Sinha,[a,b] Mohammed H. Modi,[a,b]* Haranath Ghosh,[b,c] P. K. Yadav[a] and R. K. Gupta[a]

[a]Soft X-ray Applications Laboratory, Synchrotrons Utilization Section, Raja Ramanna Centre for Advanced Technology, Indore 452013, India, [b]Homi Bhabha National Institute, Anushakti Nagar, Mumbai, Maharashtra 400094, India, and [c]Human Resource Development Section, Raja Ramanna Centre for Advanced Technology, Indore 452013, India. *Correspondence e-mail: modimh@rrcat.gov.in

Received 11 October 2017
Accepted 16 February 2018

Edited by V. Favre-Nicolin, CEA and Université Joseph Fourier, France

Keywords: synchrotron radiation; soft X-ray; magnesium compound; core-hole effect; optical property.

Supporting information: this article has supporting information at journals.iucr.org/s

The influence of the core-hole effect on optical properties of magnesium oxide (MgO) is established through experimental determination of optical constants and first-principles density functional theory studies. Optical constants (δ and β) of MgO thin film are measured in the spectral region 40–300 eV using reflectance spectroscopy techniques at the Indus-1 synchrotron radiation source. The obtained optical constants show strong core exciton features near the Mg *L*-edge region, causing significant mismatch with Henke's tabulated values. On comparing the experimentally obtained optical constants with Henke's tabulated values, an edge shift of ~3.0 eV is also observed. Distinct evidence of effects of core exciton on optical constants (δ and β) in the near Mg *L*-edge absorption spectra are confirmed through first-principles simulations.

1. Introduction

Materials that have applications in real life as well as a role in the development of fundamental sciences are most desirable. Magnesium oxide (MgO) is one such versatile material that exhibits good chemical (Luches *et al.*, 2005) and thermal stability (Wu *et al.*, 1991) along with excellent dielectric properties. Owing to its interesting properties, it is a widely used material in the emerging fields in science and technology. It is used as a barrier layer in magnetic tunnel junctions (Yuasa *et al.*, 2004; Parkin *et al.*, 2004). It is regarded as one of the potential dielectric material that has ample applications in semiconductor integrated devices. It is also well known for its use as a substrate (Awaji *et al.*, 1992) in depositing high-quality oxide films. There are several instances in the literature where MgO is regarded as a suitable material for a spacer (Fuhse *et al.*, 2004) and protective layer in multilayer mirrors in the soft X-ray/vacuum ultraviolet (VUV) region. Obtaining a fundamental understanding of the structural and optical properties of the thin film in the soft X-ray/VUV region for applications in the field of multilayer mirrors is an important requirement. Several studies are available in the literature which focus on the optical properties of technologically useful materials. However, there are very few studies available which provide unprecedented insight into the connection between optical properties and electronic structures. Recent progress in the instrumentation of the beamlines using synchrotron radiation sources enables mapping of the optical properties of materials with respect to modification in the electronic structure.

In the soft X-ray/VUV region the optical response of a material can be expressed in terms of its refractive index

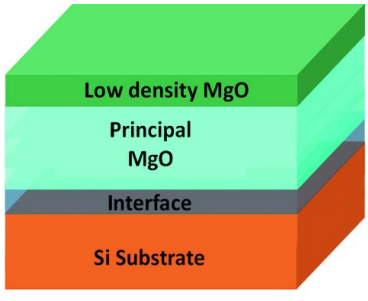

$n = 1 - \delta + i\beta$, where $(1-\delta)$ is the real part of the refractive index with δ representing dispersion and imaginary part β representing absorption. δ and β are known as optical constants. Optical properties of any material may be studied knowing the optical constants. However, the task of determining the optical constants is quite tricky in the case of compound materials, especially those having a strong core-hole effect. The weighted atomic scattering factors of the constituent elements forming the compound are used to calculate the optical constants (Henke *et al.*, 1993; Palik, 1985). This approach works satisfactorily in the energy regions away from absorption edges, whereas in the near absorption-edge region the calculated values of optical constants are found to be significantly different from the measurements, mostly because of the change in the near-neighbour environment which modifies the optical behaviour in the compound materials. In such cases experimental determination of optical constants is essential. However, in the soft X-ray region there is a scarcity of experimentally measured optical constants data. Until now the community has relied on Henke tabulated data available from CXRO (Centre for X-ray Optics; http://henke.lbl.gov/optical_constants/) which provide inaccurate data of optical constants, especially near the absorption edges. In general, there has been no satisfactory understanding achieved so far on extracting optical constants in the near-edge region of strong ionic insulators having strong core-hole effects. The main aim of this paper is a joint experiment–theory effort using a synchrotron radiation source and a computer time–space effective first-principles method.

In the X-ray region, the optical constants can be determined using techniques such as X-ray reflectivity, transmission measurements and photoemission spectroscopy using a synchrotron radiation source. Reflection spectroscopy performed in the VUV and soft X-ray region close to the *L*- and *M*-absorption edges of light and transition elements serves as a powerful tool to probe optical constants. Near the absorption edges, a strong anomalous effect perturbs the optical response. From this, additional features corresponding to the local atomic and electronic structures as obtained in near-edge X-ray absorption spectroscopy are also observed (Gibaud *et al.*, 2016). From the energy-dependent reflectivity spectra one can estimate the optical constants using the Kramers–Krönig relation (Filatova *et al.*, 1999; Sharma *et al.*, 2016) where several fine features near the edges along with small shifts may appear, which may account for core excitations and different bonding configurations, respectively.

In the literature, although electron energy-loss spectroscopy (EELS) and X-ray absorption spectroscopy (XAS) measurements of MgO are available, no reports of optical constants above the photon energy of 29 eV are available. Previously, Williams & Arakawa obtained the optical constants of MgO for the energy range 4–29 eV, by Kramers–Krönig analysis of the reflectance data (Williams & Arakawa, 1967). O'Brien *et al.* also carried out soft X-ray reflection spectroscopy measurements in the energy range 50–85 eV (O'Brien *et al.*, 1991). However, the prime inadequacy of their work was that they measured the relative reflection, not the absolute one. In this way, their information failed to provide information about the optical constants of MgO.

In this study, we present experimentally obtained optical constants of magnesium oxide (MgO) thin film in the 40–300 eV energy range covering the complete soft X-ray region available in the reflectivity beamline of the Indus-1 synchrotron radiation source. To the best of our knowledge, ours is the first experimental study which covers optical constants of MgO thin film in the wide energy range of 40–300 eV where various fine features observed in the absorption spectra near the Mg *L*-edge are explained using first-principles density functional calculations. The measured optical constants indicating the presence of fine features near the Mg *L*-edge region are compared with Henke's tabulated values obtained from the CXRO website. Henke's data do not explain the effects of the core-hole on the optical constants of MgO near the Mg absorption edge region, whereas our results provide clear evidence of the effect of the core-hole on the MgO optical constants which has been confirmed by theoretical calculations carried out under the framework of density functional theory.

2. Techniques and methods

2.1. Sample preparation

MgO thin film having a thickness of 50 nm was deposited on Si(100) substrate using the ion-beam sputtering technique. Before the deposition, the Si substrate was ultrasonically cleaned with acetone. The sputtering of pure MgO target (99.99% purity) was carried out in an argon (Ar) environment at a working pressure of 2×10^{-3} Pa. The target was sputtered with an argon ion beam having energy of 1000 V and a beam current of 30 mA. With MgO being an insulator, to avoid the sample charging effect a neutralizer was flowed at a rate of 5 sccm (sccm = standard cubic centimetres per minute). Prior to the deposition, the chamber was maintained at a base pressure of 4.2×10^{-5} Pa.

2.2. Characterization

Reflectivity measurements were performed at the reflectivity beamline of the Indus-1 synchrotron radiation source (Nandedkar *et al.*, 2002). The reflectivity beamline uses a toroidal grating monochromator to provide monochromatic photons in the 12–300 eV energy range with high flux and moderate spectral resolution ($\lambda/\Delta\lambda \simeq 200$–$450$). Different harmonic suppression edge filters are provided in the beamline to reduce higher harmonic contamination. The sample was placed at the reflectometer chamber maintained at a high vacuum of 2×10^{-5} Pa. A differential pumping system is installed to isolate the high-vacuum reflectometer from the ultra-high-vacuum section of the beamline. A θ–2θ goniometer and a linear translation stage are used for performing various scans and sample alignments. The angular resolution of the goniometer is 0.001°. The reflected beam is recorded in a soft X-ray silicon photodiode detector (International Radiation Detector Inc, USA) which has 100% internal quantum effi-

ciency. The detector signal is measured in terms of current using a Keithley electrometer (6514). Angle-dependent reflectivity measurement was carried out at an energy of 95.3 eV to determine the structural parameters. Energy-dependent reflectivity measurements were also carried out in the 40–300 eV range for a fixed glancing angle of 5°.

2.3. Methods

To determine the optical constants from the measured energy-dependent reflectivity measurements we have used a method which involves the reconstruction of the phase $\varphi(E)$ of the reflected wave from the reflectivity $R(E)$ measured for a wide energy range with the help of a dispersion relation. This dispersion relation is known as the Kramers-Krönig (KK) relation, where the phase shift can be written as (Roessler, 1965; Peiponen *et al.*, 1999)

$$\varphi(E) = -\frac{E}{\pi} P \int_0^\infty \frac{\ln R(E)}{E'^2 - E^2} \, dE', \tag{1}$$

where E is the energy of the incident photon, P represents the Cauchy principal value, R is the reflectivity and $\varphi(E)$ is the phase of the reflected electric field. The complex reflection coefficient can be written as

$$r(E) = \sqrt{R(E)} \exp[i\varphi(E)]. \tag{2}$$

In the case of *s*-polarized radiation Fresnel's reflection amplitude is expressed as

$$r_s = \frac{\sin\theta - (n^2 - \cos^2\theta)^{1/2}}{\sin\theta + (n^2 - \cos^2\theta)^{1/2}}, \tag{3}$$

where θ is the glancing angle and n is the complex index of refraction. Comparison of equations (2) and (3) gives the complex index of refraction provided that the reflectivity measurements are performed for *s*-polarized light. However, certain errors are associated with the optical constants obtained using this method due to the difficulties involved with the KK relations. The relation shown in equation (1) covers the entire range of the spectrum but, experimentally, reflectivity measurements are performed over a limited wavelength range leading to uncertainty in the determination of the phase of the reflected electric field. To minimize this error in phase, reflectivity data outside the range of measurement are extracted from the CXRO database and interpolated with our experimental data. The phase spectrum $\varphi(E)$ obtained by KK analysis of the complex reflection coefficient contains an error of $\pm\pi$ (Nash *et al.*, 1995) which is included in our analysis.

We have also carried out first-principles *ab initio* simulations employing the *CASTEP* package (Clark *et al.*, 2005) which exploits the plane-wave pseudopotential method based on density functional theory (DFT). In all of our calculations the electronic exchange-correlation is treated within the generalized gradient approximation using the Perdew–Burke–Enzerhof function (Perdew *et al.*, 1996). *CASTEP* uses a plane-wave pseudopotential approach and fast Fourier transform for the evaluation of the Hamiltonian terms. The concept of pseudopotential is a tricky one for a plane-wave basis set since the alternative all-electron potential decays too slowly to be accurately represented by a desirably small number of Fourier components. *CASTEP* offers a variety of choices for electronic relaxation and of them the density mixing method (Kresse & Furthmüller, 1996) is the most desirable. Single point energy calculations are performed for cubic Mg—O with space group symmetry $Fm\bar{3}m$ (No. 225) using on-the-fly generated pseudopotentials and a plane-wave basis set with an energy cut-off of 630 eV and self-consistent field (SCF) tolerance of 10^{-7} eV atom^{-1}. The Brillouin zone is sampled in k space within the Monkhorst–Pack scheme and the grid size for the SCF calculation is 12 × 12 × 12.

3. Results and discussion

Fig. 1 shows the angle-dependent soft X-ray reflectivity curve of MgO thin film at a photon energy of 95.3 eV along with the best fit (solid line). Analysis of the reflectivity data was carried out using the Parratt recursive formalism (Parratt, 1954), where a four-layer model was assumed consisting of a top surface low-density MgO layer, a principal MgO layer and an interfacial Mg–Si layer formed at the film/Si substrate interface along with the native oxide layer of the substrate. The effect of roughness was taken into account using the Névot–Croce model (Névot & Croce, 1980). From the analysis of the reflectivity data, the thicknesses and roughness of each layer comprising the film were evaluated along with their corresponding scattering length density (SLD). The SLD resembles the scattering power of a material. The SLD has both real and imaginary parts and it is related to the optical constants as: $\mathrm{Re}(\rho) = 2\pi\delta/\lambda^2$ and $\mathrm{Im}(\rho) = 2\pi\beta/\lambda^2$. The thicknesses and roughnesses of the top surface and principal MgO layer were found to be 3.5 and 43.4 nm and 0.95 and 0.86 nm, respectively. From the SLD (ρ) values of the top surface and principal MgO layer, it was found that the SLD of the top surface layer is 33% less than that of the principal layer. The layer model as

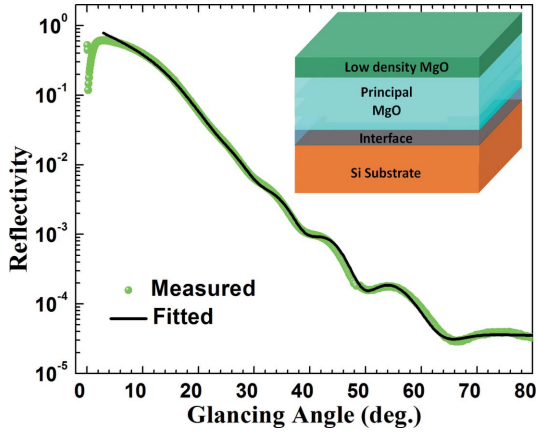

Figure 1
Measured (solid circles) and fitted (continuous line) angle-dependent soft X-ray reflectivity curve of a 500 Å-thick MgO thin film obtained using a photon energy of 95.3 eV.

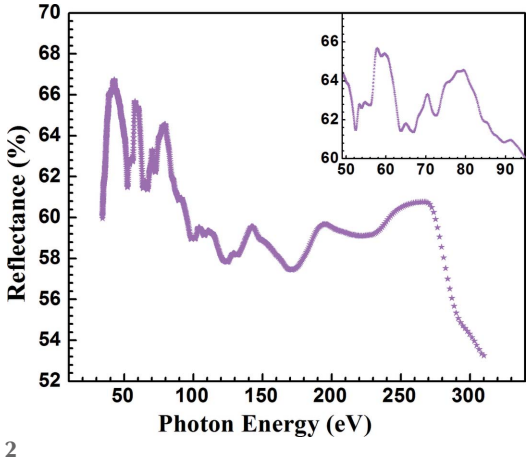

Figure 2
Measured reflectance spectrum of an MgO thin film at a fixed glancing angle of $\theta = 5^\circ$ in the energy range 40–300 eV. The inset shows the reflectance spectra neat the Mg *L*-edge.

considered for analysis was also confirmed from secondary ion mass spectrometry (SIMS) measurements. Our SIMS measurements (shown in the supporting information) also suggest that the surface layer comprises MgO, and its low density could be a result of surface roughness and the presence of unreacted oxygen *etc.* as shown from reflectivity analysis.

Fig. 2 shows the energy-dependent reflectance spectra in the 40–300 eV range for a fixed incident angle of 5°. To perform KK integration we need reflectivity data over a broader energy range (zero to infinity); thus, to satisfy this condition, we have stitched our 40–300 eV range experimental data with the calculated reflectivity data of the 300–30000 eV range and also the low-energy range. Finally the phase of the reflected wavefield was retrieved using the KK relation as shown in equation (1).

Figs. 3 and 4 show the optical constants (δ and β) of an MgO thin film obtained by applying the KK relation. The obtained optical constants over the continuous spectral range of 40–300 eV are compared with the only optical constants available from the CXRO website. The present study of optical constants measurement of MgO thin film in the 40–300 eV photon energy range has two different regions: (1) near the Mg *L*-absorption edge, 40–100 eV (as shown in the insets of Figs. 3 and 4); and (2) away from absorption edge, 100–300 eV. It is evident that the fine features are observed in the first region, *i.e.* 40–100 eV. On the other hand, no distinct features are observed in the 100–300 eV region. The features as observed in the profile of optical constants near the Mg *L*-absorption edge region are completely different from the features appearing in the Henke tabulated values. The calculation of penetration depth suggests that the photons of 40–100 eV penetrate a thickness of more than 5.0 nm and thus they interact with the principal MgO layer. This suggests that the fine features as observed in the 40–100 eV energy range are correlated with the principal MgO layer. On the other hand, in the 100–300 eV energy region the penetration depth lies within a thickness of 3.0–4.5 nm, thus representing the optical constants of the low density MgO surface layer. From the inset in Figs. 3 and 4 it is also evident that the energy position of the feature marked 'a' as determined from the experimental reflectance spectra lies at 52.8 eV which is almost consistent with O'Brien *et al.* (1991). On the other hand, according to the Henke tabulated optical constants profile obtained from CXRO database, the Mg *L*-edge is located at an energy value of 49.6 eV, which actually corresponds to that of pure Mg. This shift could be easily understood because the Henke tabulated data are calculated using the weighted sum method, and near the absorption edge region the weighted sum approach fails. For example, Mg and O atoms form an ionic bond and resultant overlapping of atomic wavefunctions leads to the formation of a new molecular wavefunction for the compound MgO. In the weighted sum approach, the role of this overlapping wavefunction is not accounted for and therefore the edge energy of the tabulated data corresponds to that of Mg.

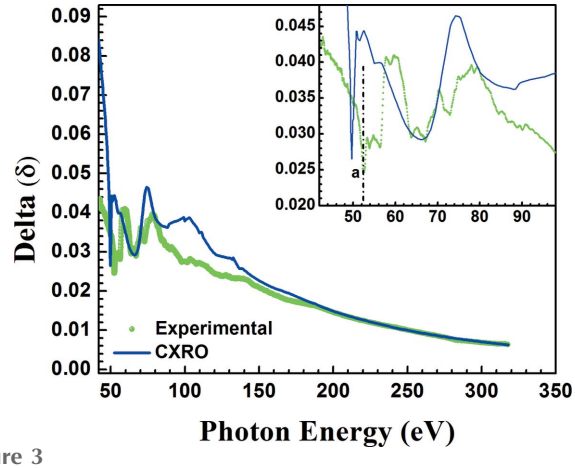

Figure 3
Measured values of δ obtained from KK analysis of reflectivity *versus* photon energy data are compared with tabulated values obtained from the CXRO database. The inset shows the 40–100 eV region where several fine features are evident.

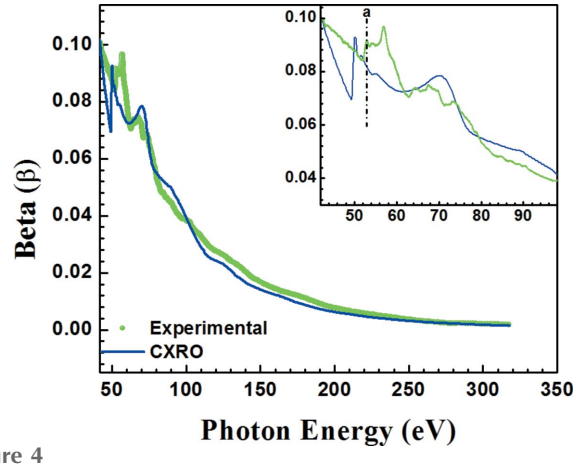

Figure 4
Measured values of β obtained from the KK analysis of reflectivity *versus* photon energy data are compared with tabulated values obtained from the CXRO database. The inset shows the 40–100 eV region where several fine features are evident.

In the experimental results, some fine features are observed in the absorption spectrum (see Fig. 4) near the Mg *L*-edge region. In our case, the appearance of fine features can be attributed to the creation of a core-exciton state as a consequence of the core-hole effect. The core-exciton states are formed owing to the Coulomb interaction between the excited electron and the core-hole formed. A detailed description of the formation of the core-exciton state is provided in the supporting information. The electron associated with a core-exciton faces an excess strong potential of the core-hole, as a result of which an observable change in the electronic structure near the vicinity of the absorption edge can be noticed. However, the strength of the core-excitonic effects may vary from system to system (*e.g.* semiconductors, insulators). In the case of MgO, the exciton is created in the band edge and it is due to the $2p^6 \rightarrow 2p^5\,3s^1$ transition in the cation site (O'Brien *et al.*, 1991). The core-exciton created leads to a modification in the oscillator strength for transitions at higher energies (Olovsson *et al.*, 2009). The creation of the core-exciton state as a result of the core-hole effect can be referred to as a modification in the electronic structure which is reflected in the optical constants profile of MgO.

In order to ensure that the fine features observed in the insets of Figs. 3 and 4 arise as a result of the presence of core-hole effects, it is necessary to provide theoretical evidence. There are several instances in the literature where core-level spectrum calculations have been carried out using different methods based on the framework of DFT. Elsässer & Köstlmeier studied the influence of supercell size on the calculated absorption spectra of MgO using the conventional $Z + 1$ approximation (Elsässer & Köstlmeier, 2001). They also generated pseudopotentials for excited states, for Mg, both with a large core (1*s*, 2*s*, 2*p* orbitals) and a small core (1*s* orbital only). The corresponding calculations were found to be in very good agreement with the results from the $Z + 1$ calculation for the Mg *K*-edge only. Hébert *et al.* carried out calculations of Mg *K*-edge absorption spectra of MgO using *WIEN2k* employing a supercell (Hébert *et al.*, 2003). In their approach the calculations were performed by removing one core electron and adding it as a uniform background charge to avoid renormalization. Olovsson *et al.* and Vinson *et al.* investigated the near-edge structure of the Mg $L_{2,3}$-edge of MgO under the framework of the Bethe–Salpeter equation (BSE) within the two-particle method (Olovsson *et al.*, 2009; Vinson *et al.*, 2011).

In this study, we have reproduced the fine features appearing in the optical constant spectra near the Mg *L*-absorption edge using first-principles calculations in *CASTEP*. Previously, Gao *et al.* carried out calculation of absorption spectra of MgO using *CASTEP*; however, their study was focused on the Mg *K*-absorption edge only (Gao *et al.*, 2009). While performing our calculations we have considered MgO to have a rocksalt cubic structure, similar to that of single-crystal MgO, and comparisons were made with the experimental absorption spectra of MgO thin film. In order to support our proposal, we have carried out total electron yield (TEY) measurements (shown in the supporting information) on both MgO thin film and substrate (single crystal) near the O *K*-edge region to compare optical constants results with single-crystal MgO. From the TEY results it was confirmed that the MgO thin film has a similar rocksalt structure to that of a single crystal. To study core-level spectroscopy using *CASTEP*, a $3 \times 3 \times 3$ supercell is used. In our approach both the advantages of reduced computational cost and the ability to study very large systems, and the accuracy of all-electron methods are retained. This is in contrast to methods such as BSE, mentioned above. Core-hole calculations are designed to describe the electronic structure of MgO containing a highly excited ion with a hole in the Mg *L*-core shell. Such calculations are relevant to the description of excitation and relaxation of these excited states. The calculations are carried out in two modes: without a core-hole and considering a core-hole on an Mg atom. Fig. 5 shows a detailed comparison of the experimental spectra with the calculated one. The 'Experimental' spectrum in Fig. 5 represents the variation of the optical constant beta (β) with respect to energy near the Mg *L*-edge. The features appearing in the spectrum are marked from 'a' to 'g'. The calculated spectrum considering the core-hole effect matches very well with the experimental one in terms of the location of these features. However, differences in terms of strength of the features in the experimental and the calculated spectra are observed. The reason behind the differences in the experimental and the calculated spectra can be attributed to the consideration of a single-crystal-like periodic system instead of the polycrystalline nature of the thin film where the presence of defects and impurities is quite expected. We have considered the width of the core-hole to be 0.25 eV in order to match the experimental spectrum. The effect of the core-hole is self evident as one compares the absorption spectra in the absence and presence of the core-hole effect. Comparing the 'Experimental' and the 'Calculated with core-hole' spectra, it is clear that the features marked as 'a' and 'b' originate as a consequence of the core hole effect. A detailed study on the various angular momentum projected partial density of states (PDOS) of MgO (shown in Fig. 6) may

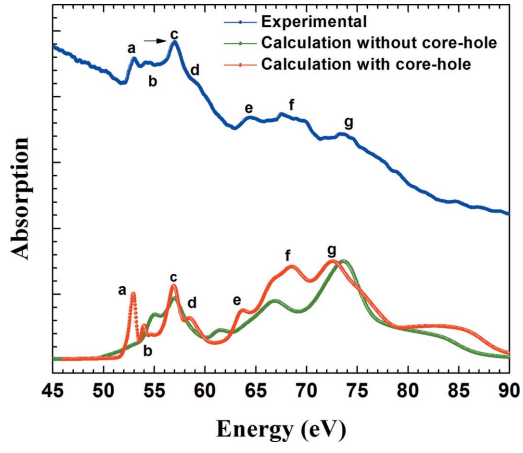

Figure 5
Experimental absorption spectra of MgO near the Mg $L_{2,3}$-edge shown along with the theoretical spectra. The experimental spectra match well with the theoretical spectra obtained by considering the core-hole effect.

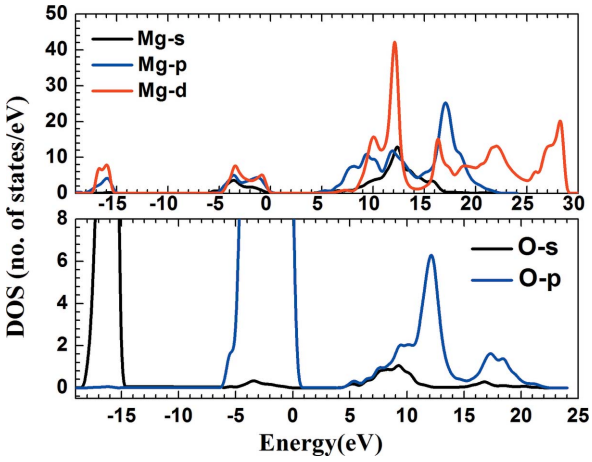

Figure 6
Calculated partial density of states (PDOS) of MgO in the absence of a core-hole.

shed significant light on this. However, it is not possible to justify the origin of every absorption feature marked from 'a' to 'g' from the calculated angular momentum projected density of states in the absence or presence of a core-hole as explained in the supporting information. In Fig. 6, the zero of the *x*-axis (energy in eV) represents the Fermi energy level. Below the Fermi energy level, the negative energy states represent the occupied energy states while the positive energy states are the unoccupied ones. Thus, from the calculated PDOS, one can conclude that the absorption features of the experimental spectrum in Fig. 5 result from the transition of Mg *p* to Mg *s*,*d* and hybridized states of Mg *s* and O *s* states, respectively. Features 'c' and 'd' originate due to the transition from Mg 2*p* to the hybridized Mg and O states, respectively. Higher-energy absorption features marked from 'e' to 'g' appear as a result of transitions to Mg 3*d* states, while the origin of the features marked as 'a' and 'b' could be explained from the calculated PDOS in the absence of a core hole. Thus, it is ensured that these two features appear as a consequence of the core-hole effect.

4. Conclusion

The influence of the core-hole effect near the Mg *L*-edge on the optical constants (δ and β) through reflectance spectroscopy and first-principles DFT studies has been conclusively demonstrated. In this work, the optical constants (δ and β) of MgO thin film in the 40–300 eV energy range obtained from reflectance spectroscopy have been reported for the first time. The optical constants are also compared with the Henke tabulated values obtained from the CXRO website. Intense features of the core-hole effect on the absorption (β) spectra of MgO obtained from first-principles simulation agree well with those of the experimentally measured values. Agreement between simulated and measured absorption (β) spectra near the Mg *L*-edge is excellent in terms of peak positions and their relative strength. Thus the core-hole effect must be considered carefully when evaluating the optical properties of MgO as well as other similar oxide materials as it influences the optical constants significantly.

Acknowledgements

The authors are thankful to Dr Mukul Gupta of UGC-DAE CSR for providing a good quality sample. HG acknowledges useful discussions with Professor Chris J Pickard.

References

Awaji, T., Sakuta, K., Sakaguchi, Y. & Kobayashi, T. (1992). *Jpn. J. Appl. Phys.* **31**, L642–L645.
Clark, S. J., Matthew, D. S., Pickard, C. J., Hasnip, P. J., Probert, M. I. J., Refson, K. & Payne, M. C. (2005). *Z. Kristallogr.* **220**, 567–570.
Elsässer, C. & Köstlmeier, S. (2001). *Ultramicroscopy*, **86**, 325–337.
Filatova, E., Lukyanov, V., Barchewitz, R., André, J.-M., Idir, M. & Stemmler, Ph. (1999). *J. Phys. Condens. Matter*, **11**, 3355–3370.
Fuhse, C., Krebs, H. U., Vitta, S. & Johansson, G. A. (2004). *Appl. Opt.* **43**, 6265–6269.
Gao, S., Pickard, C. J., Perlov, A. & Milman, V. (2009). *J. Phys. Condens. Matter*, **21**, 104203.
Gibaud, A., Bal, J. B., Gullikson, E. M., Wang, C. & Vignaud, G. (2016). *AIP Adv.* **6**, 095016.
Hébert, C., Luitz, J. & Schattschneider, P. (2003). *Micron*, **34**, 219–225.
Henke, B. L., Gullikson, E. M. & Davis, J. C. (1993). *At. Data Nucl. Data Tables*, **54**, 181–342.
Kresse, G. & Furthmüller, J. (1996). *Phys. Rev. B*, **54**, 11169–11186.
Luches, P., Benedetti, S., Liberati, M., Boscherini, F., Pronin, I. & Valeri, S. (2005). *Surf. Sci.* **583**, 191–198.
Nandedkar, R. V., Sawhney, K. J. S., Lodha, G. S., Verma, A., Raghuvanshi, V., Sinha, A. K., Modi, M. H. & Nayak, M. (2002). *Curr. Sci.* **82**, 298.
Nash, P. L., Bell, R. J. & Alexander, R. (1995). *J. Mod. Opt.* **42**, 1837–1842.
Névot, L. & Croce, P. (1980). *Rev. Phys. Appl. (Paris)*, **15**, 761–779.
O'Brien, W. L., Jia, J., Dong, Q.-Y., Callcott, T. A., Rubensson, J.-E., Mueller, D. L. & Ederer, D. L. (1991). *Phys. Rev. B*, **44**, 1013.
Olovsson, W., Tanaka, I., Mizoguchi, T., Puschnig, P. & Ambrosch-Draxl, C. (2009). *Phys. Rev. B*, **79**, 041102.
Palik, E. D. (1985). Editor. *Handbook of Optical Constants of Solids.* New York: Academic Press.
Parkin, S. S. P., Kaiser, C., Panchula, A., Rice, P. M., Hughes, B., Samant, M. & Yang, S. (2004). *Nat. Mater.* **3**, 862–867.
Parratt, L. G. (1954). *Phys. Rev.* **95**, 359–369.
Peiponen, K. E., Vartianen, E. M. & Asakura, T. (1999). *Dispersion, Complex Analysis and Optical Spectroscopy*. Berlin: Springer.
Perdew, J. P., Burke, K. & Ernzerhof, M. (1996). *Phys. Rev. Lett.* **77**, 3865–3868.
Roessler, D. M. (1965). *Br. J. Appl. Phys.* **16**, 1359.
Sharma, S., Gupta, R. K., Sinha, M., Yadav, P., Singh, A. & Modi, M. H. (2016). *AIP Conf. Proc.* **1731**, 080001.
Vinson, J., Rehr, J. J., Kas, J. J. & Shirley, E. L. (2011). *Phys. Rev. B*, **83**, 115106.
Williams, M. W. & Arakawa, E. T. (1967). *J. Appl. Phys.* **38**, 5272–5276.
Wu, M., Corneille, J. S., Estrada, C. A., He, J. & Wayne Goodman, D. (1991). *Chem. Phys. Lett.* **182**, 472–478.
Yuasa, S., Nagahama, T., Fukushima, A., Suzuki, Y. & Ando, K. (2004). *Nat. Mater.* **3**, 868–871.